

# r.sim.terrain 1.0: a landscape evolution model with dynamic hydrology

Brendan Alexander Harmon<sup>1</sup>, Helena Mitasova<sup>2,3</sup>, Anna Petrasova<sup>2,3</sup>, and Vaclav Petras<sup>2,3</sup>

<sup>1</sup>Robert Reich School of Landscape Architecture, Louisiana State University, Baton Rouge, Louisiana, USA

<sup>2</sup>Center for Geospatial Analytics, North Carolina State University, Raleigh, North Carolina, USA

<sup>3</sup>Department of Marine, Earth, and Atmospheric Sciences, North Carolina State University, Raleigh, North Carolina, USA

**Correspondence:** Brendan Harmon (baharmon@lsu.edu)

**Abstract.** While there are numerical landscape evolution models that simulate how steady state flows of water and sediment reshape topography over long periods of time, r.sim.terrain is the first to simulate short-term topographic change for both steady state and dynamic flow regimes across a range of spatial scales. This free and open source, GIS-based topographic evolution model uses empirical models for soil erosion at watershed to regional scales and a physics-based model for shallow overland water flow and soil erosion at subwatershed scales to compute short-term topographic change. This model uses either a steady state or dynamic representation of overland flow to simulate how overland sediment mass flows reshape topography for a range of hydrologic soil erosion regimes based on topographic, land cover, soil, and rainfall parameters. As demonstrated by a case study for Patterson Branch subwatershed on the Fort Bragg military installation in North Carolina, r.sim.terrain simulates the development of fine-scale morphological features including ephemeral gullies, rills, and hillslopes. Applications include land management, erosion control, landscape planning, and landscape restoration.

*Copyright statement. ...*

## 1 Introduction

Landscape evolution models represent how the surface of the earth changes over time in response to physical processes. Most studies of landscape evolution have been descriptive, but a number of numerical landscape evolution models have been developed that simulate elevational change over time (Temme et al., 2013). Numerical landscape evolution models such as the Channel-Hillslope Integrated Landscape Development (CHILD) model (Tucker et al., 2001), SIBERIA (Willgoose, 2005), LAPSUS (Schoorl et al., 2000, 2002), and the GRASS GIS add-on module r.landscap.evol (Barton et al., 2010) simulate steady state flows over long temporal scales. Landlab, a new Python library for numerically modeling Earth surface processes (Hobley et al., 2017), has components for simulating landscape evolution such as the Stream Power with Alluvium Conservation and Entrainment (SPACE) model (Shobe et al., 2017). While Geographic Information Systems (GIS) support efficient data management, spatial and statistical modeling and analysis, and visualization, there are few GIS-based soil erosion models

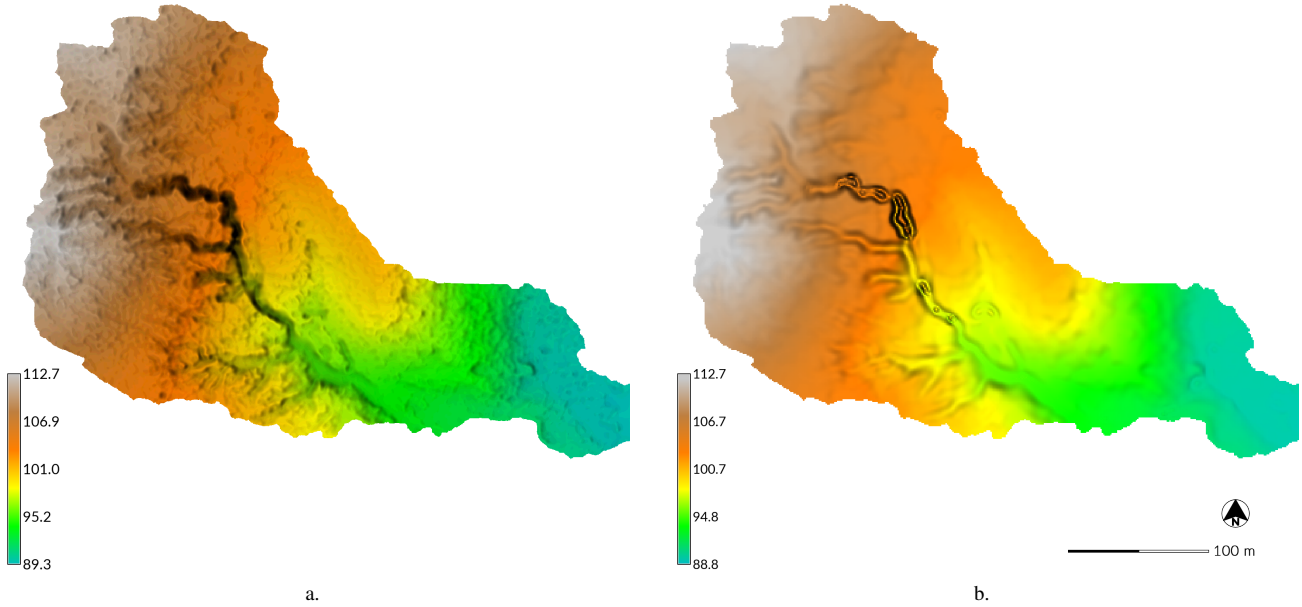


**Figure 1.** The digital elevation model (DEM) (a) before and (b) after simulated landscape evolution with r.sim.terrain for a subwatershed of Patterson Branch, Fort Bragg, NC, USA. (a) The before DEM was generated from an airborne lidar survey in 2012. This simulation used the SIMWE model for a 120 min rainfall event with  $50 \text{ mm hr}^{-1}$  for a variable erosion-deposition regime at steady state. (b) In the evolved DEM the gully channel has widened with depositional ridges forming along its thalweg.

(see Table 1) or landscape evolution models. Furthermore there are still major research questions to address in the theoretical foundations of erosion modeling such as how erosional processes scale over time and space and how sediment detachment and transport interact (Mitasova et al., 2013). While most numerical landscape evolution models simulate peak flows at steady state, short-term erosional processes like gully formation can be dynamic with significant morphological changes happening within minutes before flows reach steady state. A landscape evolution model with dynamic water and sediment flow is needed to study fine-scale spatial and short-term temporal erosional processes such as gully formation and the development of microtopography.

At the beginning of a rainfall event the overland water flow regime is dynamic – its depth changes at a variable rate over time and space. If the intensity of rainfall continues to change throughout the event then the flow regime will remain dynamic. If, however, the overland flow reaches a peak rate then the hydrologic regime is considered to be at steady state. At steady state:

$$\frac{\partial h(x, y, t)}{\partial t} = 0 \quad (1)$$

where:

$(x, y)$  is the position [m]

$t$  is the time [s]

$h(x, y, t)$  is the depth of overland flow [m]

- Gullies are eroded, steep banked channels formed by ephemeral, concentrated flows of water. A gully forms when overland
- 5 waterflow converges in a knickzone – a concave space with steeper slopes than its surroundings (Zahra et al., 2017) – during intense rainfall events. When the force of the water flow concentrated in the knickzone is enough to detach and transport large amounts of sediment, an incision begins to form at the apex of the knickzone – the knickpoint or headwall. As erosion continues the knickpoint begins to migrate upslope and the nascent gully channel widens, forming steep channel banks. Multiple incisions initiated by different knickpoints may merge into a gully channel and multiple channels may merge into a branching
- 10 gully system (Mitasova et al., 2013). This erosive process is dynamic; the morphological changes drive further changes in a positive feedback loop. When the gully initially forms the soil erosion regime should be detachment capacity limited with the concentrated flow of water in the channel of the gully detaching large amounts of sediment and transporting it to the foot of the gully, potentially forming a depositional fan. If the intensity of rainfall decreases and transport and detachment capacity approach a balance, then the soil erosion regime may switch to in which soil is eroded and deposited in a spatially variable pattern.
- 15 Subsequent rainfall events may trigger further knickpoint formation and upslope migration, channel incision and widening, and depositional fan and ridge formation. Between high intensity rainfall events, lower intensity events and gravitational diffusion may gradually smooth the shape of the gully. Eventually, if detachment capacity significantly exceeds transport capacity and the regime switches to transport capacity limited, the gully may fill with sediment, as soil continues to be eroded, but is not transported far.
- 20 Gully erosion rates and evolution can be monitored in the field or modeled on the computer. Field methods include dendrogeomorphology (Malik, 2008) and permanent monitoring stakes for recording erosion rates, extensometers for recording mass wasting events, weirs for recording water and suspended sediment discharge rates, and time series of surveys using total station theodolites (Thomas et al., 2004), unmanned aerial systems (UAS) (Jeziorska et al., 2016; Kasprak et al., 2019; Yang et al., 2019), airborne lidar (Perroy et al., 2010; Starek et al., 2011), and terrestrial lidar (Starek et al., 2011; Bechet et al.,
- 25 2016; Goodwin et al., 2016; Telling et al., 2017). With terrestrial lidar, airborne lidar, and UAS photogrammetry there is now sufficient resolution topographic data to morphometrically analyze and numerically model fine-scale landscape evolution in GIS including processes such as gully formation and the development of microtopography. Gully erosion has been simulated with RUSLE2-Raster (RUSLER) in conjunction with the Ephemeral Gully Erosion Estimator (EphGEE) (Dabney et al., 2014), while gully evolution has been simulated for detachment capacity limited erosion regimes with the Simulation of Water Erosion (SIMWE) model (Koco, 2011; Mitasova et al., 2013). Now numerical landscape evolution models that can simulate steady state and dynamic flow regimes and switch between soil erosion regimes are needed to study fine-scale spatial and short-term temporal erosional processes.

The numerical landscape evolution model r.sim.terrain was developed to simulate the spatiotemporal evolution of landforms caused by shallow overland water and sediment flows at spatial scales ranging from square meters to kilometers and temporal

35 scales ranging from minutes to years. This open source, GIS-based landscape evolution model can model steady state or

dynamic flow regimes for different soil erosion regimes and simulate the evolution of fine-scale morphological features such as ephemeral gullies (Figure 2). It was designed as a research tool for studying how erosional processes scale over time and space, comparing empirical and process-based models, comparing steady state and dynamic flow regimes, and studying the role of dynamic flow regimes in fine-scale morphological change. r.sim.terrain was tested with a subwatershed scale (450 m<sup>2</sup>)  
5 case study and the simulations were compared against a time-series of airborne lidar surveys.

## 2 r.sim.terrain

The process-based, spatially distributed landscape evolution model r.sim.terrain simulates topographic changes caused by shallow, overland water flow across a range of spatiotemporal scales and soil erosion regimes using either the Simulated Water Erosion (SIMWE) model, the 3-Dimensional Revised Universal Soil Loss Equation (RUSLE 3D) model, or the Unit Stream Power Erosion Deposition (USPED) model. The r.sim.terrain model can simulate either steady state or dynamic flow regimes.  
10 SIMWE is a physics-based simulation that uses a Monte Carlo path sampling method to solve the water and sediment flow equations (Mitas and Mitasova, 1998; Mitasova et al., 2004). With SIMWE r.sim.terrain uses the modeled flow of sediment – a function of water flow and soil detachment and transport parameters – to estimate net erosion and deposition rates. RUSLE3D is an empirical equation for estimating soil erosion rates in detachment capacity limited soil erosion regimes (Mitasova et al.,  
15 1996, 2013). With RUSLE3D r.sim.terrain uses an event-based rainfall erosivity factor, soil erodibility factor, landcover factor, and 3D topographic factor – a function of slope and flow accumulation – to model soil erosion rates. USPED is a semi-empirical equation for net erosion and deposition in transport capacity limited soil erosion regimes (Mitasova et al., 1996, 2013). With USPED r.sim.terrain uses an event-based rainfall erosivity factor, soil erodibility factor, landcover factor, and a 3D topographic factor to model net erosion or deposition rates as the divergence of sediment flows. For each of the models topographic change  
20 is derived at each time step from the erosion rate or net erosion-deposition rate and gravitational diffusion.

The r.sim.terrain model can simulate the evolution of gullies including processes such as knickpoint migration, channel incision, channel widening, aggradation, and scour pool and depositional ridge formation along the thalweg of the gully. Applications include geomorphological research, erosion control, landscape restoration, and scenario development for landscape planning and management. This model can simulate landscape evolution over a wide range of spatial scales from  
25 small watersheds less than ten square kilometers with SIMWE to regional watersheds of hundreds of square kilometers with USPED or RULSE3D, although it does not model fluvial processes. It has been used at resolutions ranging from sub-meter to 30 m. The model has been implemented as a Python add-on module for the free, open source Geographic Resources Analysis Support System (GRASS) GIS (GRASS Development Team). The source code is available at [https://github.com/baharmon/landscape\\_evolution](https://github.com/baharmon/landscape_evolution) under the GNU General Public License v2. It supports multithreading and parallel processing to efficiently compute simulations using large, high resolution topographic datasets. The landscape evolution model can be installed in GRASS GIS as an add-on module with the command:  
30

```
g.extension extension=r.sim.terrain
```

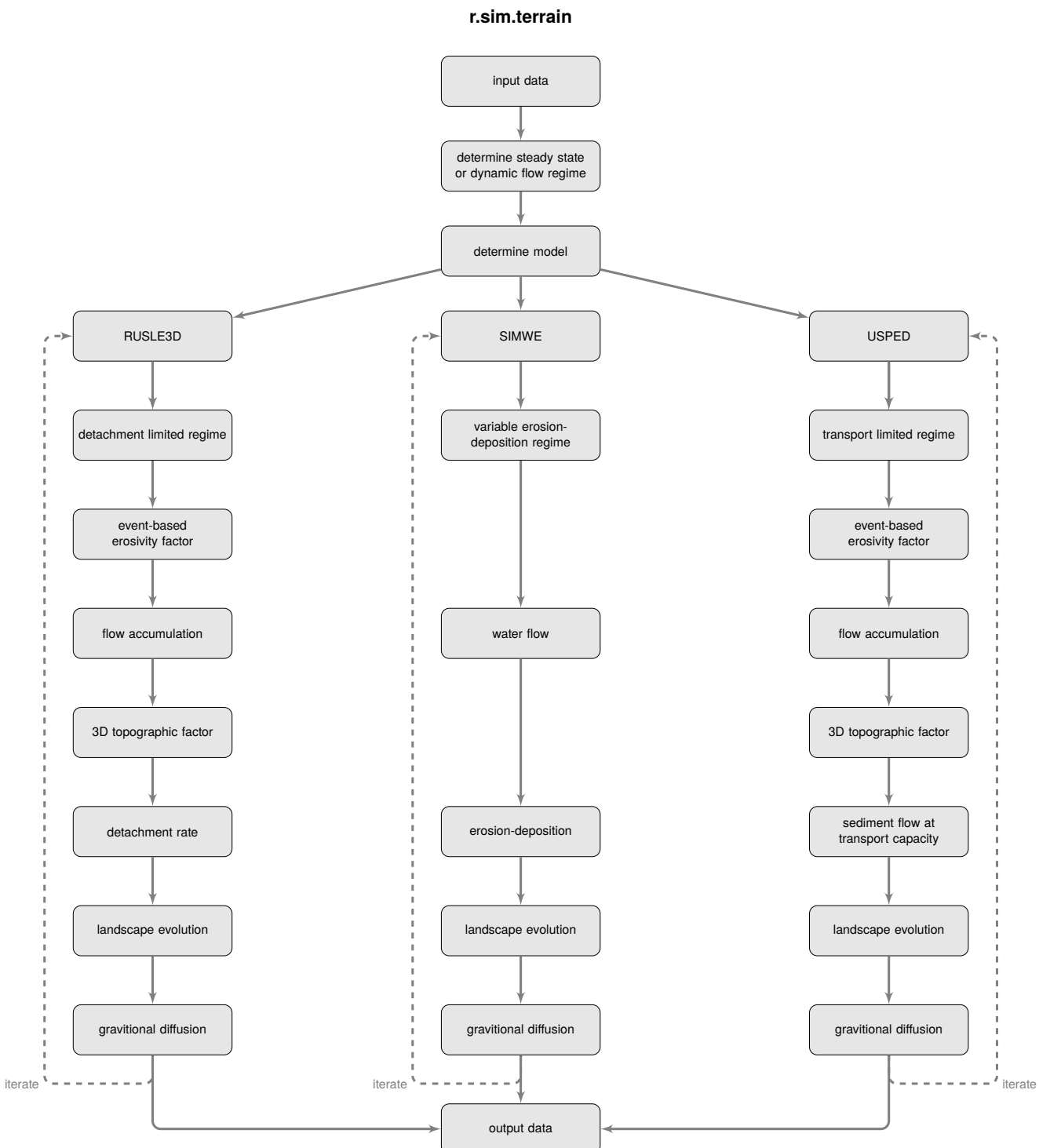


**Figure 2.** Conceptual diagram for `r.sim.terrain`.

**Table 1.** Geospatial soil erosion models

Model	Spatial scale	Temporal scale	Representation	Implementation	Reference
RUSLE3D	regional	continuous	raster	map algebra	(Mitasova et al., 1996)
USPED	watershed	continuous	raster	map algebra	(Mitasova et al., 1996)
SIMWE	watershed	event – continuous	raster	GRASS modules	(Mitas and Mitasova, 1998)
GeoWEPP	watershed	continuous	raster	ArcGIS module	(Flanagan et al., 2013)
AGWA	watershed	event – continuous	vector	ArcGIS module	(Guertin et al., 2015)
openLISEM	watershed	event	raster	PCRaster script	(Roo et al., 1996)
Landlab	watershed	event – continuous	raster + mesh	Python library	(Hobley et al., 2017)

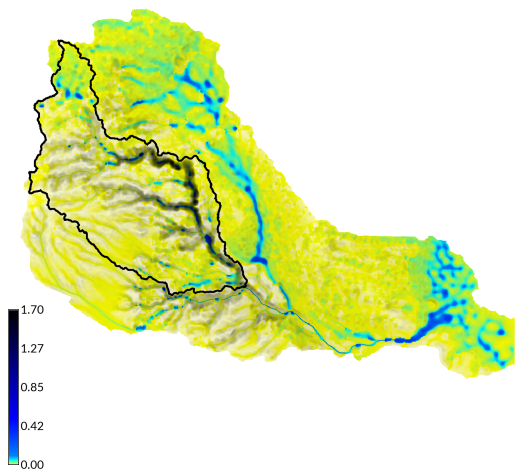
Limitations of this landscape evolution model include shallow overland flow, units, computation time, resolution and spatial scale. `r.sim.terrain` only models shallow overland flows, not fluvial processes or subsurface flows. It requires data – including elevation and rainfall intensity – in metric units. The SIMWE model is computationally intensive and may require long computation times even with multithreading. Because SIMWE uses a Green's function Monte Carlo solution of the sediment transport equation, the accuracy, detail, and smoothness of the results depend on the number of random walkers. While a large number of random walkers will reduce the numerical error in the path sampling solution, it will also greatly increase computation time. Furthermore a customized compilation of GRASS GIS is needed for more than 7 million random walkers. This limits the resolution and spatial scale at which SIMWE can be easily applied, while RUSLE3D and USPED are much faster, computationally efficient, and can easily be run at regional scales.

## 10 2.1 Landscape evolution

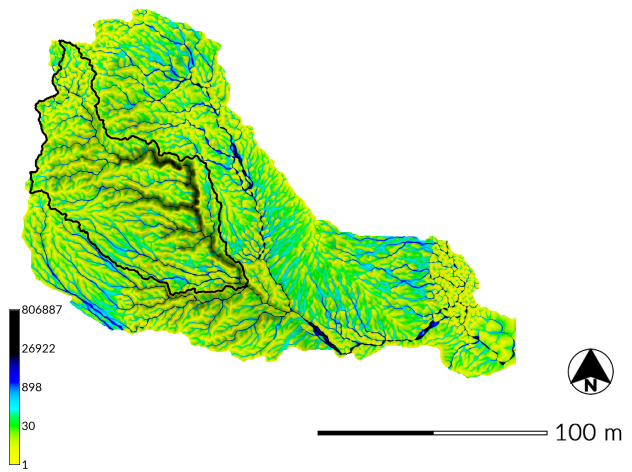
The simulated change in elevation over time  $\partial z / \partial t$  [m s<sup>-1</sup>] is a function of the net erosion-deposition rate  $d_s$  [kg m<sup>-2</sup> s<sup>-1</sup>] and the sediment mass density  $\rho_s$  [kg m<sup>-3</sup>] (Mitasova et al., 2013):

$$\frac{\partial z}{\partial t} = d_s \rho_s^{-1} \quad (2)$$

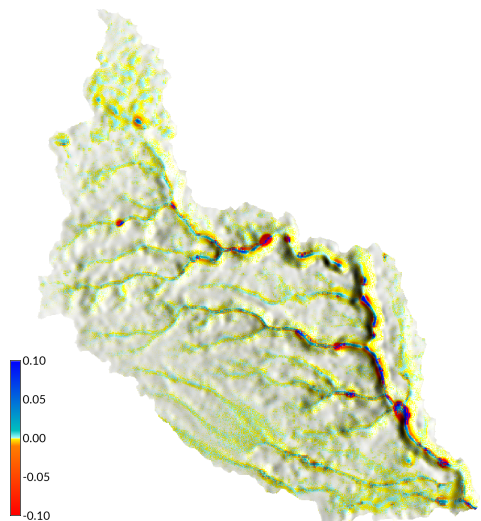
The net erosion-deposition rate  $d_s$  can be estimated at different levels of complexity based on the user selected simulation mode guided by the type of application. The simulation modes include the process-based SIMWE model for steady state and dynamic shallow overland flow and variable erosion-deposition regime, USPED model for the transport capacity limited regime or RUSLE3D model for the detachment capacity limited case. In the detachment capacity limited regime, there is no deposition and  $d_s$  represents soil erosion rate (soil loss). Gravitational diffusion is then applied to the evolved topography to simulate smoothing effects of localized transport of soil that occurs during and between rainfall events. The simulated change



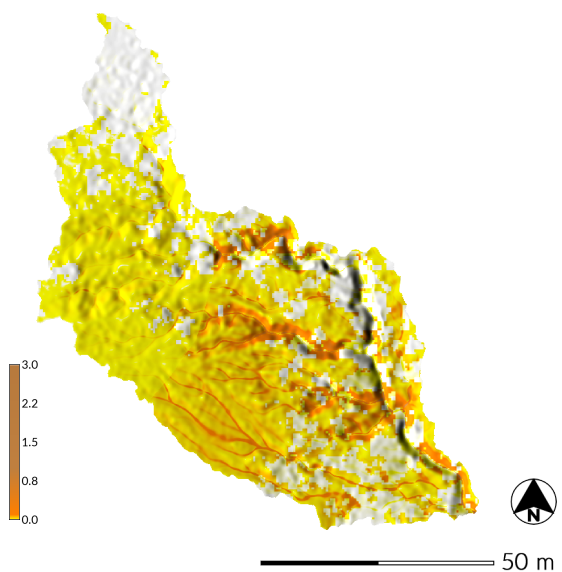
a.



b.



c.



d.

**Figure 3.** Water and sediment flows modeled by (a & c) SIMWE and (b & d) RUSLE3D with spatially variable landcover for a (a & b) subwatershed and (c & d) drainage area of Patterson Branch, Fort Bragg, NC at 0.3 m resolution. (a) Water depth [m] simulated by SIMWE for a 10 min event with  $50 \text{ mm hr}^{-1}$  in the subwatershed. (b) Flow accumulation for RUSLE3D in the subwatershed. (c) Erosion and deposition [ $\text{kg m}^{-2} \text{ s}^{-1}$ ] simulated by SIMWE in drainage area 1. (d) Erosion [ $\text{kg m}^{-2} \text{ s}^{-1}$ ] modeled by RUSLE3D in drainage area 1.

in elevation  $\partial z / \partial t$  due to gravitational diffusion is a function of the the sediment mass density, the diffusion coefficient, and Laplacian of the elevation (Thaxton, 2004):

$$\frac{\partial z}{\partial t} = \rho_s^{-1} \varepsilon_g \nabla^2 z \quad (3)$$

where  $\varepsilon_g$  is the diffusion coefficient [ $\text{m}^2 \text{ s}^{-1}$ ].

## 5 2.2 Simulation of Water Erosion (SIMWE)

SIMWE is a physics-based simulation of shallow overland water and sediment flow that uses a path sampling method to solve the continuity and momentum equations with a 2D diffusive wave approximation (Mitas and Mitasova, 1998; Mitasova et al., 2004). SIMWE has been implemented in GRASS GIS as the modules r.sim.water and r.sim.sediment. In SIMWE mode for each time step r.sim.terrain computes the first order partial derivatives of elevation, simulates shallow water flow and net erosion-deposition ( $d_s$ ), and then evolves the topography based on the erosion-deposition rate and gravitational diffusion. The model simulates dynamic flow regimes when the time step is less than the travel time for a drop of water or a particle of sediment to cross the landscape. With longer time steps the model simulates a steady state regime. In SIMWE the erosion regime is determined by the balance of the sediment detachment capacity ( $D_c$ ) and the sediment transport capacity ( $T_c$ ) represented by the first order reaction term  $\sigma$ , which depends on soil and landcover properties. The detachment capacity is the maximum potential detachment rate by overland flow, while the sediment transport capacity is the maximum potential sediment flow rate (Mitasova and Mitas, 2001).

$$\sigma = \frac{D_c}{T_c} \quad (4)$$

where:

$\sigma$  is a first order reaction term [ $\text{m}^{-1}$ ]

20  $D_c$  is the sediment detachment capacity [ $\text{kg m}^{-1} \text{s}^{-1}$ ]

$T_c$  is the sediment transport capacity [ $\text{kg m}^{-1} \text{s}^{-1}$ ]

### 2.2.1 Shallow water flow

The SIMWE model simulates shallow overland water flow controlled by spatially variable topographic, soil, landcover, and rainfall parameters by solving the continuity and momentum equations for steady state water flow with a path sampling method (Fig. 3a). Shallow water flow  $q$  can be approximated by the bivariate form of the St. Venant equation:

$$\frac{\partial h}{\partial t} = i_e - \nabla \cdot q \quad (5)$$

where:

$x, y$  is the position [m]

30  $t$  is the time [s]

$h$  is the depth of overland flow [m]

$i_e$  is the rainfall excess [ $\text{m s}^{-1}$ ]

(i.e. rainfall intensity – infiltration – vegetation intercept)

$\nabla$  is the divergence of the flow vector field

5  $q$  is the water flow per unit width [ $\text{m}^2 \text{s}^{-1}$ ].

Diffusive wave effects can be approximated so that water can flow through depressions by integrating a diffusion term  $\propto \nabla^2[h^{5/3}]$  into the solution of the continuity and momentum equations for steady state water flow. This equation is solved using a Green's function Monte Carlo path sampling method.

10 
$$-\frac{\varepsilon}{2} \nabla^2[h^{5/3}] + \nabla[h v] = i_e \quad (6)$$

where:

$\varepsilon$  is a spatially variable diffusion coefficient.

### 2.2.2 Erosion-deposition

15 In SIMWE the net erosion-deposition rate is estimated using the bivariate form of sediment continuity equation to model sediment storage and flow based on effective sources and sinks (Fig. 3c). Net erosion-deposition  $d_s$  – the difference between sources and sinks – is approximated by the steady state sediment flow equation with diffusion:

$$d_s = \frac{\partial[\rho_s h]}{\partial t} + \nabla q_s \quad (7)$$

where:

20  $d_s$  is net erosion-deposition [ $\text{kg m}^{-2} \text{s}^{-1}$ ].

### 2.2.3 Landscape evolution

The simulated change in elevation  $\Delta z$  due to water erosion and deposition is a function of the change in time, the net erosion-deposition rate, and the sediment mass density (Mitasova et al., 2013):

25 
$$\Delta z = \Delta t d_s \rho_s^{-1} \quad (8)$$

Gravitational diffusion is then applied to the evolved topography to simulate the settling of sediment particles. The simulated change in elevation  $\Delta z$  due to gravitational diffusion is a function of the change in time, the sediment mass density, the gravitational diffusion coefficient, and topographic divergence – i.e. the sum of the second order derivatives of elevation (Thaxton, 2004):

30 
$$\Delta z = \Delta t \rho_s^{-1} \varepsilon_g \nabla \quad (9)$$

where:

$\varepsilon_g$  is the gravitational diffusion coefficient [ $\text{m}^2 \text{ s}^{-1}$ ]

$\nabla$  is the topographic divergence [ $\text{m}^{-1}$ ].

## 5 2.3 Revised Universal Soil Loss Equation for Complex Terrain (RUSLE3D)

RUSLE3D is an empirical equation for computing erosion in a detachment capacity limited soil erosion regime for watersheds with complex topography (Mitasova et al., 1996). It is based on the Universal Soil Loss Equation (USLE), an empirical equation for estimating the average sheet and rill soil erosion from rainfall and runoff on agricultural fields and rangelands with simple topography (Wischmeier et al., 1978). It models erosion dominated regimes without deposition in which sediment  
10 transport capacity is uniformly greater than detachment capacity. As an empirical equation the predicted soil loss is spatially and temporally averaged. In USLE soil loss per unit area is determined by an erosivity factor  $R$ , a soil erodibility factor  $K$ , a slope length factor  $L$ , a slope steepness factor  $S$ , a cover management factor  $C$ , and a prevention measures factor  $P$ . These factors are empirical constants derived from an extensive collection of measurements on 22.13 m standard plots with an average slope of 9%. RUSLE3D was designed to account for more complex, 3D topography with converging and diverging flows. In  
15 RUSLE3D the topographic potential for erosion at any given point is represented by a 3D topographic factor  $LS_{3D}$ , which is a function of the upslope contributing area and the angle of the slope.

In this spatially and temporally distributed model RUSLE3D is modified by the use of an erosivity factor derived from the rainfall intensity at each time step. For each time step this model computes the parameters for RUSLE3D – an event-based erosivity factor, the slope of the topography, the flow accumulation, and the 3D topographic factor – and then solves the  
20 RUSLE3D equation for sediment flow. The sediment flow is used to simulate landscape evolution in a detachment capacity limited soil erosion regime.

### 2.3.1 Erosivity factor

The erosivity factor  $R$  in USLE and RUSLE is the combination of the total energy and peak intensity of a rainfall event, representing the interaction between the detachment of sediment particles and the transport capacity of the flow. It can be  
25 calculated as the product of the kinetic energy of the rainfall event  $E$  and its maximum 30 min intensity  $I_{30}$  (Brown and Foster, 1987; Renard et al., 1997). The erosivity of a single rainfall event  $EI_{30}$  divided into  $m$  total periods can be calculated as (Panagos et al., 2015, 2017):

$$EI_{30} = \left( \sum_{r=1}^m e_r v_r \right) I_{30} \quad (10)$$

where:

30  $EI_{30}$  is the rainfall erosivity index of a single event [ $\text{MJ mm ha}^{-1} \text{ hr}^{-1}$ ]

$e_r$  is the unit rainfall energy [ $\text{MJ ha}^{-1} \text{ mm}^{-1}$ ]

$v_r$  is the rainfall volume [mm] during time period  $r$

$I_{30}$  is the maximum rainfall intensity during a 30-min period of the rainfall event [ $\text{mm hr}^{-1}$ ].

In this model, however, the erosivity factor is derived at each time step  $r$  as a function of kinetic energy ( $e_r$ ), rainfall volume ( $v_r$ ), rainfall intensity ( $i_r$ ). First rain energy is derived from rainfall intensity (Brown and Foster, 1987):

$$5 \quad \frac{e_r}{e_0} = 1. - a \exp(i_0 i_r) \quad (11)$$

where:

$i_r$  is rainfall intensity [ $\text{mm h}^{-1}$ ]

$a = 0.72$  is an empirical coefficient

$i_0 = -0.05$  is an exponent.

10 Then the erosivity per time step is calculated as the product of unit rain energy, rainfall volume, rainfall intensity, and time:

$$EI_r = e_r v_r i_r \quad (12)$$

where:

$EI_r$  is the rainfall erosivity during time  $r$  [ $\text{MJ mm ha}^{-1} \text{ hr}^{-1}$ ].

### 2.3.2 Flow accumulation

15 The upslope contributing area per unit width  $a$  is determined by flow accumulation times grid cell width (Fig. 3d). Flow accumulation is calculated using a multiple flow direction algorithm (Metz et al., 2009) based on  $A^T$  least cost path searches (Ehlschlaeger, 1989). The multiple flow direction algorithm implemented in GRASS GIS as the module r.watershed is computationally efficient and can navigate nested depressions and other obstacles.

### 2.3.3 3D topographic factor

20 The 3D topographic factor  $LS_{3D}(x, y)$  is calculated as a function of flow accumulation, representing the upslope contributing area and the slope (Fig. 3e). The empirical coefficients  $m$  and  $n$  for the upslope contributing area and the slope can range from 0.2 to 0.6 and 1.0 to 1.3 respectively with low values representing dominant sheet flow and high values representing dominant rill flow.

$$LS_{3D} = (m + 1.0) (a(x, y) a_0^{-1})^m (\sin(\beta) \beta_0^{-1})^n \quad (13)$$

25 where:

$LS_{3D}$  is the dimensionless topographic (length-slope) factor

$a$  is upslope contributing area per unit width [m]

$a_0$  is the length of the standard USLE plot [22.1 m]

$\beta$  is the angle of the slope [ $^\circ$ ]

30  $m$  is an empirical coefficient

$n$  is an empirical coefficient

$\beta_0$  is the slope of the standard USLE plot [0.09°]

### 2.3.4 Detachment limited erosion rate

- 5 The detachment limited erosion rate is a function of the erosivity factor, the soil erodibility factor, the 3D topographic factor, cover factor, and the prevention measures factor (Fig. 3f):

$$E = R K LS_{3D} C P \quad (14)$$

where:

$E$  is the detachment rate [ton ha<sup>-1</sup> yr<sup>-1</sup>]

10  $R$  is the rainfall erosivity factor [MJ mm ha<sup>-1</sup> hr<sup>-1</sup> yr<sup>-1</sup>]

$K$  is the soil erodibility factor [ton ha hr ha<sup>-1</sup> MJ<sup>-1</sup> mm<sup>-1</sup>]

$LS_{3D}$  is the dimensionless topographic (length-slope) factor

$C$  is the dimensionless land cover factor

$P$  is the dimensionless prevention measures factor.

15

With RUSLE3D the simulated change in elevation  $\Delta z$  is derived from equation 8 for landscape evolution and then the equation 9 for the settling of sediment particles due to gravitational diffusion.

### 2.4 Unit Strempower Erosion Deposition (USPED)

USPED estimates net erosion-deposition as the divergence of sediment flow in transport capacity limited soil erosion regimes.

- 20 At transport capacity shallow flows of water are carrying as much sediment possible – more sediment is being detached than can be transported. As a transport capacity limited model USPED predicts erosion where transport capacity increases and deposition where transport capacity decreases. The influence of topography on erosion and deposition in USPED is represented by a topographic sediment transport factor, while the influence of soil and landcover are represented by factors adopted from USLE and RUSLE (Mitasova et al., 1996). Net erosion-deposition is estimated by computing the event-based erosivity factor  
25 ( $R_e$ ) using Eq. 12, the slope and aspect of the topography, the flow accumulation with a multiple flow direction algorithm, the topographic sediment transport factor, the sediment flow at transport capacity, and the divergence of the sediment flow.

The 3D topographic factor (Eq. 13) for RUSLE3D is adapted to represent the topographic sediment transport factor ( $LST$ ) – the topographic component of overland flow at sediment transport capacity:

$$LST = a^m (\sin \beta)^n \quad (15)$$

30 where:

$LST$  is the topographic sediment transport factor

*a* is the upslope contributing area per unit width [m]

*β* is the angle of the slope [°]

*m* is an empirical coefficient

*n* is an empirical coefficient.

5

The sediment flow at transport capacity is a function of the event-based rainfall factor, the soil erodibility factor, the topographic component of overland flow, the landcover factor, and the prevention measures factor:

$$T = R_e K C P LST \quad (16)$$

where:

10 *T* is sediment flow at transport capacity [ton ha<sup>-1</sup> yr<sup>-1</sup>]

*R* is the rainfall erosivity factor [MJ mm ha<sup>-1</sup> hr<sup>-1</sup> yr<sup>-1</sup>]

*K* is the soil erodibility factor [ton ha hr ha<sup>-1</sup> MJ<sup>-1</sup> mm<sup>-1</sup>]

*C* is the dimensionless land cover factor

*P* is the dimensionless prevention measures factor.

15

Net erosion-deposition at transport capacity is estimated as the divergence of sediment flow:

$$d_s = \frac{\partial(T \cos \alpha)}{\partial x} + \frac{\partial(T \sin \alpha)}{\partial y} \quad (17)$$

where:

*d<sub>s</sub>* is net erosion-deposition [kg m<sup>-2</sup> s<sup>-1</sup>]

20 *α* is the aspect of the topography [°].

With USPED the simulated change in elevation  $\Delta z$  is derived from equation 8 for landscape evolution and then equation 9 for the settling of sediment particles due to gravitational diffusion.

### 3 Case study

25 Military activity is a high-impact land use that can cause significant physical alteration to the landscape. Erosion is a major concern for military installations, particularly at training bases, where the land surface is disturbed by off-road vehicles, foot traffic, and munitions. Off-road vehicles and foot traffic by soldiers cause the loss of vegetative cover, the disruption of soil structure, soil compaction, and increased runoff due to reduced soil capacity for water infiltration (Webb and Wilshire, 1983; McDonald, 2004).

20 Gullies – ephemeral channels with steep headwalls that incise into unconsolidated soil to depths of meters – are a manifestation of erosion common to military training installations like Ft. Bragg in North Carolina and the Piñon Canyon Maneuver Site in Colorado. While the local development of gullies can restrict the maneuverability of troops and vehicles

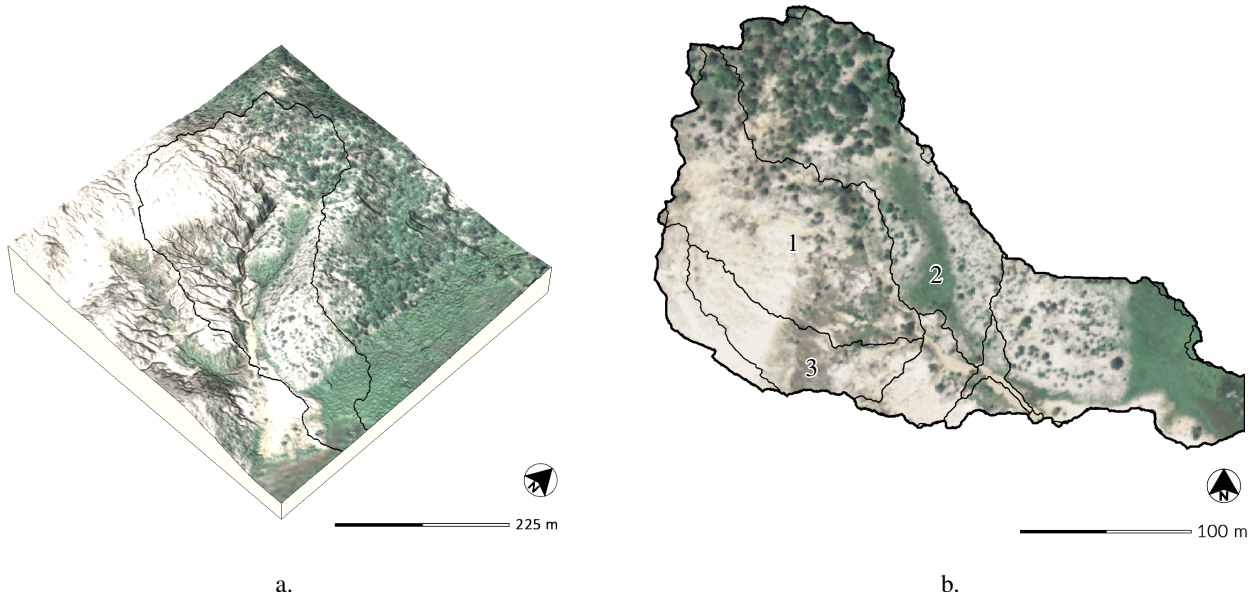


**Figure 4.** Subwatershed with 2014 orthoimagery (a) draped over the 2016 digital elevation model and (b) drainage areas with 2014 orthoimagery, Patterson Branch, Fort Bragg, NC, USA

during training exercises, pervasive gullying across a landscape can degrade an entire training area (Huang and Niemann, 2014).

To test the effectiveness of the different models in r.sim.terrain we compared the simulated evolution of a highly eroded subwatershed of Patterson Branch on Fort Bragg, North Carolina against a timeseries of airborne lidar surveys. The models –  
5 SIMWE, RUSLE3D, and USPED – were tested in steady state and dynamic modes for constant rainfall, design storms, and recorded rainfall.

### 3.1 Patterson Branch

With 650 km<sup>2</sup> of land Fort Bragg is the largest military installation in the US and has extensive areas of bare, erodible soils on impact areas, firing ranges, landing zones, and dropzones. It is located in the Sandhills region of North Carolina with a Longleaf Pine and Wiregrass Ecosystem (Sorrie et al., 2006). The study landscape – a subwatershed of Patterson Branch (Figure 4a) in the Coleman Impact Area – is pitted with impact craters from artillery and mortar shells and has an active, approximately 2 m deep gully. It is a Pine-Scrub Oak Sandhill community composed primarily of Longleaf Pine (*Pinus palustris*) and Wiregrass (*Aristida stricta*) on Blaney and Gilead loamy sands (Sorrie, 2004). Throughout the Coleman Impact Area frequent fires ignited by live munitions drive the ecological disturbance regime of this fire adapted ecosystem. In 2016 the 450 m<sup>2</sup> study site was  
10 15 43.24% bare ground with predominately loamy sands, 39.54% covered by the Wiregrass community, and 17.22% forested with

the Longleaf Pine community (Figure 5a). We hypothesize that the elimination of forest cover in the impact zone triggered extensive channelized overland flow, gully formation, and sediment transport into the creek.

Timeseries of digital elevations models and landcover maps for the study landscape were generated from lidar pointclouds and orthophotography. The digital elevations models for 2004, 2012, and 2016 were interpolated at 0.3 m resolution using the 5 regularized spline with tension function (Mitasova and Mitas, 1993; Mitasova et al., 2005) from airborne lidar surveys collected by the NC Floodplain Mapping program and Fort Bragg. Unsupervised image classification was used to identify clusters of spectral reflectance in a timeseries of 1 m resolution orthoimagery collected by the National Agriculture Imagery Program. The landcover maps were derived from the classified lidar point clouds and the classified orthoimagery. Spatially variable soil erosion factors – k-factor, c-factor, manning's, and runoff rates – were then derived from the landcover and soil maps. The 10 dataset for this study is hosted at [https://github.com/baharmon/landscape\\_evolution\\_dataset](https://github.com/baharmon/landscape_evolution_dataset) under the ODC Open Database License (ODbL). The data is derived from publicly available data from the US Army, USGS, USDA, Wake County GIS, NC Floodplain Mapping Program, and the NC State Climate Office. There are detailed instructions for preparing the input data in the tutorial and a complete record of the commands used to process the sample data in the data log.

We used the geomorphons method of automated landform classification based on the openness of terrain (Jasiewicz and 15 Stepinski, 2013) and the difference between the digital elevation models to analyze the changing morphology of the study area (Figure 5c-d). The 2 m deep gully – its channels classified as valleys and its scour pits as depressions by geomorphons – has multiple mature branches and ends with a depositional fan. The gully has also developed depositional ridges beside the channels. Deep scour pits have developed where branches join the main channel and where the main channel has sharp bends. A new branch has begun to form in a knickzone classified as a mix of valleys and hollows on a grassy swale on the northeast 20 side of the gully. Between 2012 and 2016 a depositional ridge has developed at the foot of this nascent branch where it would meet the main channel. The difference in elevation between 2012 and 2016 (Figure 5b) shows a deepening of the main channel by approximately 0.2 m and the scours pits by approximately 1 m, while depositional ridges have formed and grown up to approximately 1 m or more.

### 3.2 Simulations

25 We ran a sequence of r.sim.terrain simulations with design storms for the Patterson Branch subwatershed study area to demonstrate the capabilities of the RUSLE3D, USPED, and SIMWE models (Table 2). To analyze the results of the simulations, we compared net differences in elevation morphological features, and linear regressions of elevation change.

While r.sim.terrain can use rainfall records, we used design storms to demonstrate and test the basic capabilities of the model. Our design storms are based off the peak rainfall values in records from the State Climate Office of North Carolina. We 30 used RUSLE3D to simulate landscape evolution in a dynamic, detachment capacity limited soil erosion regime for a 120 min design storm with 3 min intervals and a constant rainfall intensity of  $50 \text{ mm hr}^{-1}$  (Figure 7a-b). We used USPED to simulate landscape evolution in a dynamic, transport capacity limited soil erosion regime for a 120 min design storm with 3 min intervals and a constant rainfall intensity of  $50 \text{ mm hr}^{-1}$  (Figure 7c-d). We used SIMWE to simulate landscape evolution in a steady state, variable erosion-deposition soil erosion regime for a 120 min design storm with a constant rainfall intensity of

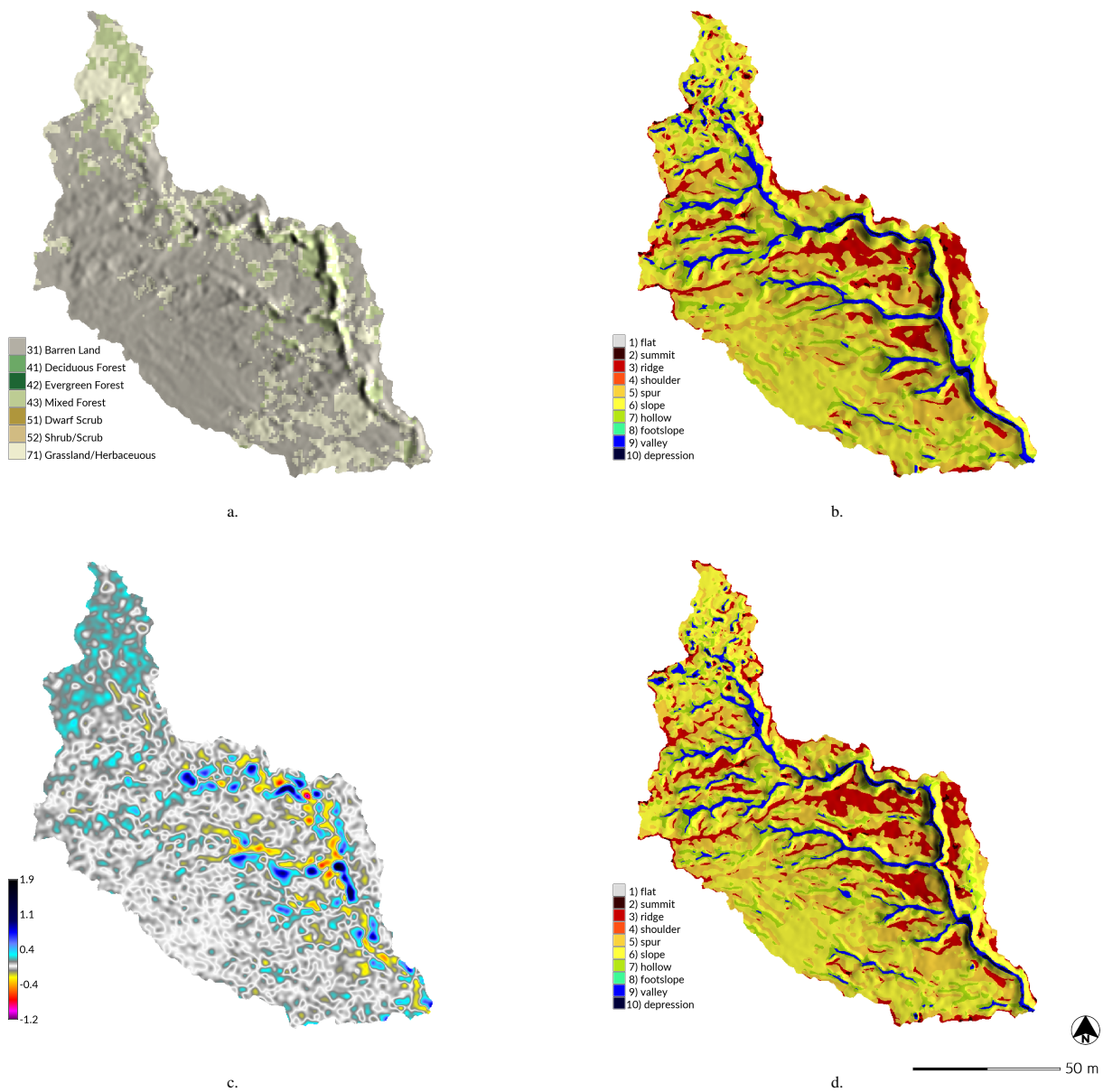


**Figure 5.** Morphological Change, Drainage Area 1, Study Subwatershed, Patterson Branch, Fort Bragg, NC, USA. (a) Landcover in 2014, (b) landforms in 2012, (c) elevation difference between 2012-2016 [m], and (d) landforms in 2016.

**Table 2.** Landscape evolution simulations

Flow regime	Model	Intensity	Duration	Interval	m	n	$\rho_s$	Threads	Runtime
Dynamic	RUSLE3D	50 mm hr <sup>-1</sup>	120 min	3 min	0.4	1.3			2 min 36 s
Dynamic	USPED	50 mm hr <sup>-1</sup>	120 min	3 min	1.5	1.2	1.6		3 min 14 s
Steady state	SIMWE	50 mm hr <sup>-1</sup>	120 min	120 min			1.6	6	44 min 51 s

**Table 3.** Linear regression of elevation maps for drainage area

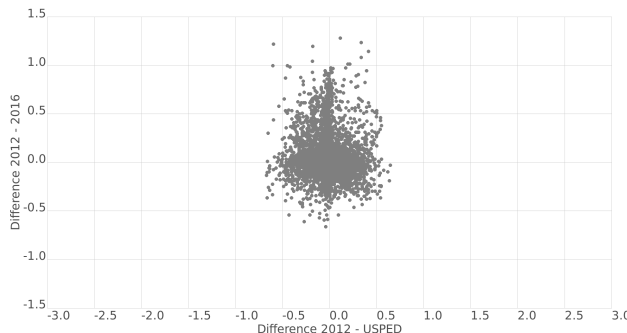
Elevation A	Elevation B	Correlation coeff. (R)	Difference in R from 2012-2016 baseline
2012	2016	0.999490	0
2012	simulated with RUSLE3D	0.999848	-0.000483
2012	simulated with USPED	0.999973	-0.000253
2012	simulated with SIMWE	0.998312	0.001178

50 mm hr<sup>-1</sup> (Figure 8a-b). In all of the simulations a sink filling algorithm – an optional parameter in r.sim.terrain – was used to reduce the effects of positive feedback loops that cause the over-development of scour pits.

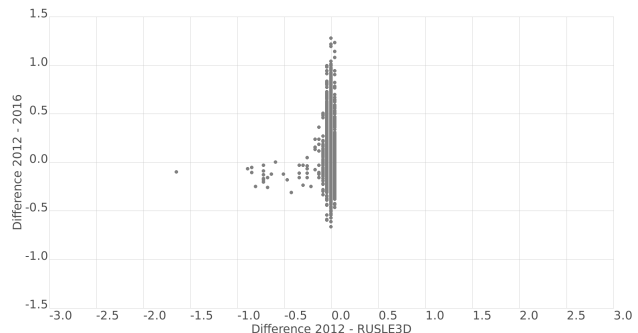
The simulations were automated and run in parallel using Python scripts that are available in the software repository. The simulations can be reproduced using these scripts and the study area dataset by following the instructions in the Open Science Framework repository at <https://osf.io/tf6yb/>. The simulations were run in GRASS GIS 7.4 on a desktop computer with 64-bit Ubuntu 16.04.4 LTS, 8 x 4.20 GHz Intel Core i7 7700K CPUs, and 32 GB RAM. Simulations using SIMWE are far more computationally intensive than RULSE3D or USPED, but support multi-threading when compiled with OpenMP. Dynamic simulations of RUSLE3D and USPED took 2 min 36 s and 3 min 14 s respectively to run on a single thread, while the steady state simulation for SIMWE took 44 min 51 s running on 6 threads (Table 2).

### 10 3.3 Results

The dynamic RUSLE3D simulation deepened the main channel of the gully, while the dynamic USPED simulation eroded the banks of the gully and deposited in channels causing the gully grow wider and shallower (Figure 7). As a detachment capacity limited model RUSLE3D's results were dominated by erosion and thus negative elevation change. RUSLE3D carved a deep incision in the main gully channel where water accumulated (Figure 7b). As a transport capacity limited model USPED generated a distributed pattern with both erosion and deposition and thus negative and positive elevation change. While USPED's pattern of elevation change was grainy and fragmented, it captured the process of channel filling and widening expected with a transport capacity limited soil erosion regime (Figure 7d). The steady state SIMWE simulation for a variable erosion-deposition regime



a.



b.

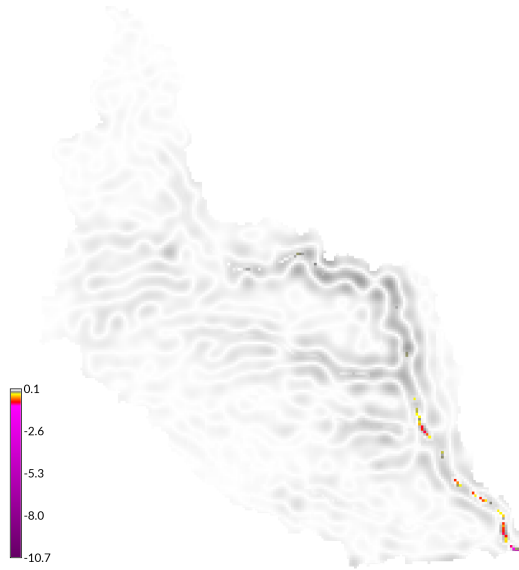
**Figure 6.** Bivariate scatterplots of observed change in elevation from 2012-2016 versus the change simulated with (a) USPED and (b) RUSLE3D.

predicted the morphological processes and features expected of its regime including gradual aggradation, channel widening, and the formation of depositional ridges along the thalweg of the channel (Figure 8b).

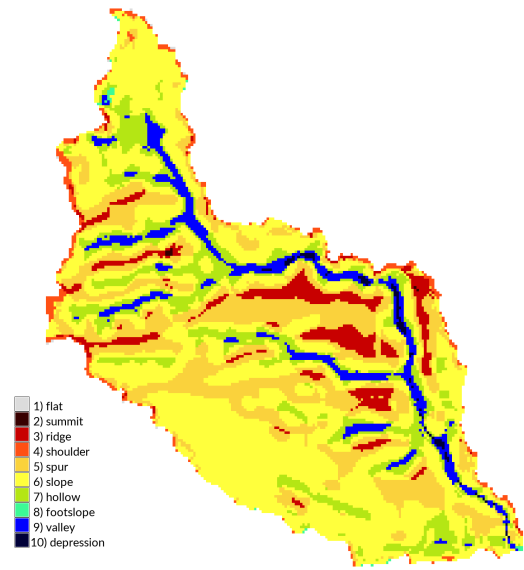
We used linear regressions to quantitatively analyze observed versus simulated changes in topographic elevation (Table 3 & Figure 6). The results of the USPED simulation closely fit the observed change in elevation between 2012-2016, while 5 RUSLE3D overpredicted erosion and SIMWE overpredicted deposition. While USPED generated a grainy pattern of erosion and deposition, it was much faster than SIMWE, most closely fit the observed change, and simulated the key morphological patterns and processes – channel incision, filling, and widening. Given their speed and approximate modeling of erosive processes, RUSLE3D and USPED are effective for simulating landscape evolution on large rasters. RUSLE3D for example has been used to model erosion for the entire 650 km<sup>2</sup> Fort Bragg installation at 9 m resolution (Levine et al., 2018).

## 10 4 Conclusions

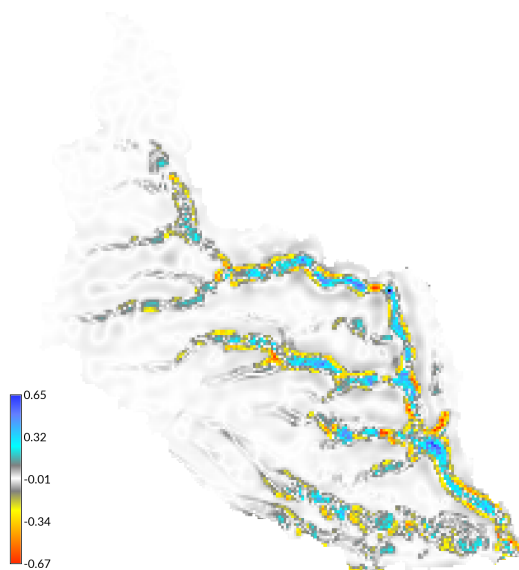
The short-term landscape evolution model `r.sim.terrain` can simulate the development of gullies, rills, and hillslopes by overland water erosion for a range of hydrologic and soil erosion regimes. The landscape evolution model was tested with a series of simulations for different hydrologic and soil erosion regimes for a highly eroded sub-watershed on Fort Bragg with an active gully. For each regime it generated the morphological processes and features expected. The physics-based SIMWE model 15 simulated morphological processes for a variable erosion-deposition regime such as gradual aggradation, channel widening, scouring, and the development of depositional ridges along the thalweg. The empirical RUSLE3D and USPED models approximated short-term topographic change at watershed to regional scales. The empirical RUSLE3D model simulated channel incision in a detachment limited soil erosion regime, while the empirical USPED model simulated channel widening and filling in a transport limited regime. The elevation change simulated with the USPED model most closely fit the observed change in 20 the study landscape. Since `r.sim.terrain` is a GIS-based model that simulates fine-scale morphological processes and features, it can easily and effectively be used in conjunction with other GIS-based tools for geomorphological research, land management



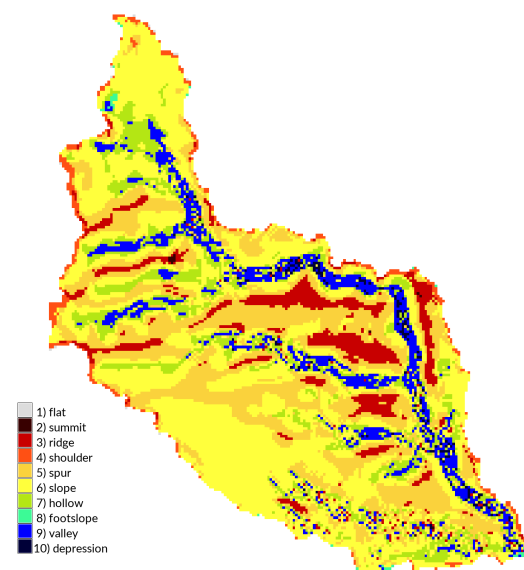
a.



b.



c.



d.



**Figure 7.** Dynamic simulations with (a-b) RUSLE3D and (c-d) USPED for a 120 min event with a rainfall intensity of  $50 \text{ mm hr}^{-1}$  at 1 m resolution for Drainage Area 1, Study Subwatershed, Patterson Branch, Fort Bragg, NC. The (a) net difference [m] and (b) landforms for the RUSLE3D simulation. The (c) net difference [m] and (d) landforms for the USPED simulation.

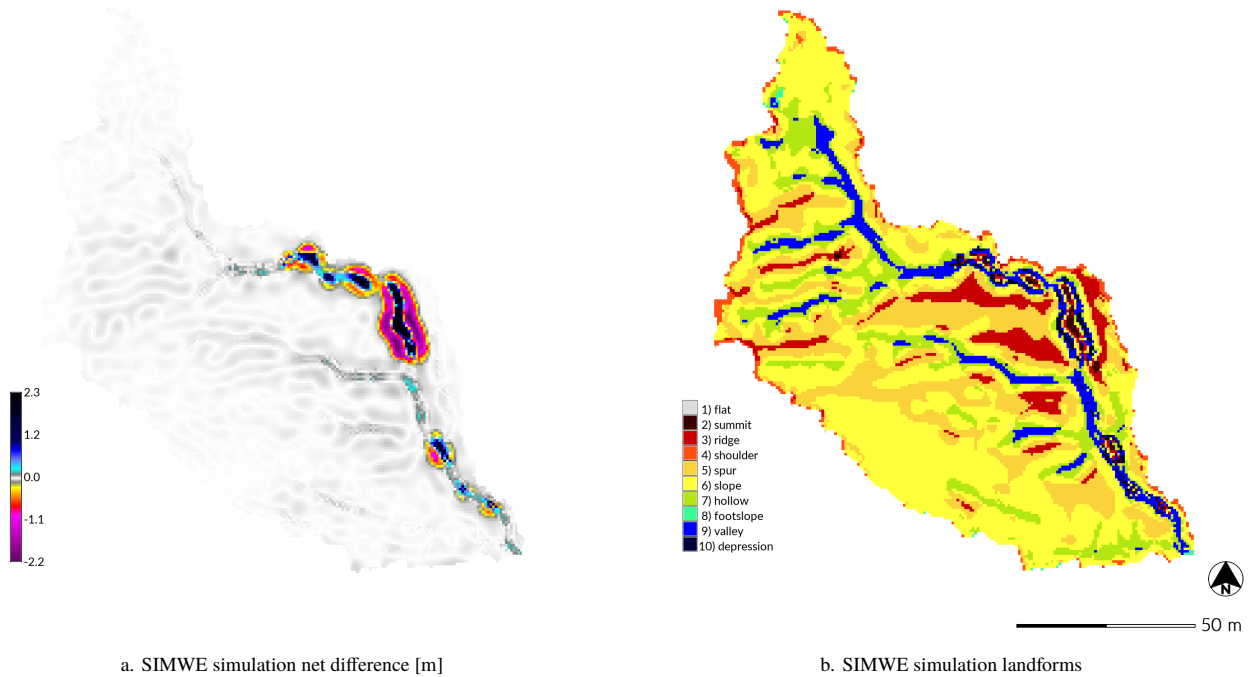


**Figure 8.** The (a) net difference [m] and (b) landforms simulated with SIMWE at steady state for a 120 min event with a rainfall intensity of  $50 \text{ mm hr}^{-1}$  at 1 m resolution for Drainage Area 1, Study Subwatershed, Patterson Branch, Fort Bragg, NC.

and conservation, erosion control, and landscape restoration. In the future we plan to assess this model by comparing simulations against a monthly timeseries of submeter resolution surveys by unmanned aerial systems and terrestrial lidar. We also plan to develop a case study demonstrating how the model can be used as a planning tool for landscape restoration. Planned enhancements to model include modeling subsurface flows, accounting for bedrock, and a reverse landscape evolution mode  
5 for backward modeling.

*Code and data availability.* As a work of open science this study is reproducible, repeatable, and recomputable. Since the data, model, GIS, dependencies are all free and open source, the study can easily be reproduced. The landscape evolution model has been implemented in Python as module for GRASS GIS, a free and open source GIS. The source code for the model is hosted on GitHub at [https://github.com/baharmon/landscape\\_evolution](https://github.com/baharmon/landscape_evolution) under the GNU General Public License version 2. The code repository also includes Python scripts for  
10 running and reproducing the simulations in this paper. The digital object identifier (DOI) for the version of the software documented in this paper is: <https://doi.org/10.5281/zenodo.2542921>. There are detailed instructions for running this model in the manual at <https://grass.osgeo.org/grass76/manuals/addons/r.sim.terrain.html> and the tutorial at [https://github.com/baharmon/landscape\\_evolution/blob/master/tutorial.md](https://github.com/baharmon/landscape_evolution/blob/master/tutorial.md). The geospatial dataset for the study area is available on GitHub at [https://github.com/baharmon/landscape\\_evolution\\_dataset](https://github.com/baharmon/landscape_evolution_dataset) under the Open Database License with the DOI: <https://doi.org/10.5281/zenodo.2542929>. The data log has a complete record of the commands used to

process the sample data. The source code, scripts, data, and results are also hosted on the Open Science Framework at <https://osf.io/tf6yb/> with the DOI: <https://doi.org/10.17605/osf.io/tf6yb>.

*Author contributions.* Brendan Harmon developed the models, code, data, case studies, and manuscript. Helena Mitasova contributed to the development of the models and case studies and revised the manuscript. Anna Petrasova and Vaclav Petras contributed to the development  
5 of the code. All authors read and approved the final manuscript.

*Competing interests.* The authors declare that they have no conflict of interest.

*Acknowledgements.* We acknowledge the GRASS GIS Development Community for developing and maintaining GRASS GIS.

## References

- Barton, C. M., Ullah, I., and Mitasova, H.: Computational Modeling and Neolithic Socioecological Dynamics: a Case Study from Southwest Asia, *American Antiquity*, 75, 364–386, <http://www.jstor.org/stable/25766199>, 2010.
- Bechet, J., Duc, J., Loyer, A., Jaboyedoff, M., Mathys, N., Malet, J. P., Klotz, S., Le Bouteiller, C., Rudaz, B., and Travelletti, J.: Detection of seasonal cycles of erosion processes in a black marl gully from a time series of high-resolution digital elevation models (DEMs), *Earth Surface Dynamics*, 4, 781–798, <https://doi.org/10.5194/esurf-4-781-2016>, 2016.
- 5 Brown, L. C. and Foster, G. R.: Storm Erosivity Using Idealized Intensity Distributions, *Transactions of the American Society of Agricultural Engineers*, 30, 0379 –0386, <https://doi.org/http://dx.doi.org/10.13031/2013.31957>, 1987.
- Dabney, S., Vieira, D., Bingner, R., Yoder, D., and Altinakar, M.: Modeling Agricultural Sheet , Rill and Ephemeral Gully Erosion, in: ICHE 10 2014. Proceedings of the 11th International Conference on Hydroscience & Engineering, pp. 1119–1126, Karlsruhe, 2014.
- Ehlschlaeger, C.: Using the A<sup>T</sup> Search Algorithm to Develop Hydrologic Models from Digital Elevation Data, in: Proceedings of International Geographic Information Systems (IGIS) Symposium '89, pp. 275–281, Baltimore, MD, 1989.
- Flanagan, D. C., Frankenberger, J. R., Cochrane, T. A., Renschler, C. S., and Elliot, W. J.: Geospatial Application of the Water Erosion Prediction Project (WEPP) Model, *Transactions of the ASABE*, 56, 591–601, <https://doi.org/10.13031/2013.42681>, <https://www.fs.usda.gov/treesearch/pubs/43830>, 2013.
- 15 Goodwin, N. R., Armston, J., Stiller, I., and Muir, J.: Assessing the repeatability of terrestrial laser scanning for monitoring gully topography: A case study from Aratula, Queensland, Australia, *Geomorphology*, 262, 24 – 36, <https://doi.org/https://doi.org/10.1016/j.geomorph.2016.03.007>, <http://www.sciencedirect.com/science/article/pii/S0169555X16300976>, 2016.
- 20 GRASS Development Team: GRASS GIS, <https://grass.osgeo.org>.
- Guertin, D. P., Goodrich, D. C., Burns, I. S., Korgaonkar, Y., Barlow, J., Sheppard, B. S., Unkrich, C., and Kepner, W.: Automated Geospatial Watershed Assessment Tool (AGWA), <https://doi.org/10.1061/9780784479322.012>, 2015.
- Hobley, D. E., Adams, J. M., Siddhartha Nudurupati, S., Hutton, E. W., Gasparini, N. M., Istanbulluoglu, E., and Tucker, G. E.: Creative computing with Landlab: An open-source toolkit for building, coupling, and exploring two-dimensional numerical models of Earth-surface 25 dynamics, *Earth Surface Dynamics*, 5, 21–46, <https://doi.org/10.5194/esurf-5-21-2017>, 2017.
- Huang, X. and Niemann, J. D.: Simulating the impacts of small convective storms and channel transmission losses on gully evolution, in: Military Geosciences in the Twenty-First Century, edited by Harmon, R. S., Baker, S. E., and McDonald, E. V., Geological Society of America, [https://doi.org/10.1007/978-1-4020-3105-2\\_18](https://doi.org/10.1007/978-1-4020-3105-2_18), 2014.
- Jasiewicz, J. and Stepinski, T. F.: Geomorphons - a pattern recognition approach to classification and mapping of landforms, *Geomorphology*, 30 182, 147–156, <https://doi.org/10.1016/j.geomorph.2012.11.005>, 2013.
- Jeziorska, J., Mitasova, H., Petrasova, A., Petras, V., Divakaran, D., and Zajkowski, T.: Overland Flow analysis using times series of sUAS-derived elevation models, in: ISPRS Annals of the Photogrammetry, Remote Sensing and Spatial Information Sciences, vol. 3, pp. 159–166, <https://doi.org/10.5194/isprs-annals-III-8-159-2016>, 2016.
- Kasprak, A., Bransky, N. D., Sankey, J. B., Caster, J., and Sankey, T. T.: The effects of topographic surveying technique and data resolution on the detection and interpretation of geomorphic change, *Geomorphology*, 333, 1 – 15, <https://doi.org/https://doi.org/10.1016/j.geomorph.2019.02.020>, <http://www.sciencedirect.com/science/article/pii/S0169555X19300546>, 2019.

- Koco, Š.: Simulation of gully erosion using the SIMWE model and GIS, *Landsurface Analysis*, 17, 81–86, 2011.
- Levine, J., Wegmann, K., Mitasova, H., Eads, C., Lyons, N., Harmon, B., McCarter, C., Peart, S., Oberle, N., and Walter, M.: Freshwater Bivalve Survey for Endangered Species Branch Fort Bragg, NC, Tech. rep., North Carolina State University, Raleigh, NC, <https://doi.org/10.13140/RG.2.2.17512.11521>, 2018.
- 5 Malik, I.: Dating of small gully formation and establishing erosion rates in old gullies under forest by means of anatomical changes in exposed tree roots (Southern Poland), *Geomorphology*, 93, 421–436, <https://doi.org/10.1016/j.geomorph.2007.03.007>, 2008.
- McDonald, K. W.: Military Foot Traffic Impact on Soil Compaction Properties, pp. 229–242, Springer Netherlands, Dordrecht, [https://doi.org/10.1007/978-1-4020-3105-2\\_18](https://doi.org/10.1007/978-1-4020-3105-2_18), 2004.
- Metz, M., Mitasova, H., and Harmon, R. S.: Fast Stream Extraction from Large , Radar- Based Elevation Models with Variable Level of 10 Detail, pp. 237–242, 2009.
- Mitas, L. and Mitasova, H.: Distributed soil erosion simulation for effective erosion prevention, *Water Resources Research*, 34, 505–516, <https://doi.org/10.1029/97wr03347>, 1998.
- Mitasova, H. and Mitas, L.: Interpolation by regularized spline with tension: I. Theory and implementation, *Mathematical Geology*, 25, 641–655, <https://doi.org/10.1007/BF00893171>, 1993.
- 15 Mitasova, H. and Mitas, L.: Multiscale soil erosion simulations for land use management, in: *Landscape erosion and evolution modeling*, edited by Harmon, R. S. and Doe, W. W., chap. 11, pp. 321–347, Springer, Boston, MA, [https://doi.org/10.1007/978-1-4615-0575-4\\_11](https://doi.org/10.1007/978-1-4615-0575-4_11), 2001.
- Mitasova, H., Hofierka, J., Zlocha, M., and Iverson, L. R.: Modelling topographic potential for erosion and deposition using GIS, *International Journal of Geographical Information Science*, 10, 629–641, <https://doi.org/10.1080/02693799608902101>, <http://dx.doi.org/10.1080/02693799608902101>, 1996.
- 20 Mitasova, H., Thaxton, C., Hofierka, J., McLaughlin, R., Moore, A., and Mitas, L.: Path sampling method for modeling overland water flow, sediment transport, and short term terrain evolution in Open Source GIS, *Developments in Water Science*, 55, 1479–1490, [https://doi.org/10.1016/S0167-5648\(04\)80159-X](https://doi.org/10.1016/S0167-5648(04)80159-X), 2004.
- Mitasova, H., Mitas, L., and Harmon, R. S.: Simultaneous spline approximation and topographic analysis for lidar elevation data in open- 25 source GIS, *IEEE Geoscience and Remote Sensing Letters*, 2, 375–379, <https://doi.org/10.1109/LGRS.2005.848533>, 2005.
- Mitasova, H., Barton, M., Ullah, I., Hofierka, J., and Harmon, R.: 3.9 GIS-Based Soil Erosion Modeling, in: *Treatise on Geomorphology*, edited by Shroder, J. F., chap. 3.9, pp. 228–258, Elsevier, San Diego, California, USA, <https://doi.org/10.1016/B978-0-12-374739-6.00052-X>, <http://www.sciencedirect.com/science/article/pii/B978012374739600052X>, 2013.
- Panagos, P., Ballabio, C., Borrelli, P., Meusburger, K., Klik, A., Rousseva, S., Tadić, M. P., Michaelides, S., Hrabalíková, M., Olsen, P., 30 Aalto, J., Lakatos, M., Rymszewicz, A., Dumitrescu, A., Beguería, S., and Alewell, C.: Rainfall erosivity in Europe, *Science of the Total Environment*, 511, 801–814, <https://doi.org/10.1016/j.scitotenv.2015.01.008>, 2015.
- Panagos, P., Borrelli, P., Meusburger, K., Yu, B., Klik, A., Jae Lim, K., Yang, J. E., Ni, J., Miao, C., Chattopadhyay, N., Sadeghi, S. H., Hazbavi, Z., Zabihi, M., Larionov, G. A., Krasnov, S. F., Gorobets, A. V., Levi, Y., Erpul, G., Birkel, C., Hoyos, N., Naipal, V., Oliveira, P. T. S., Bonilla, C. A., Meddi, M., Nel, W., Al Dashti, H., Boni, M., Diodato, N., Van Oost, K., Nearing, M., and Ballabio, C.: Global rainfall 35 erosivity assessment based on high-temporal resolution rainfall records, *Scientific Reports*, 7, 4175, <https://doi.org/10.1038/s41598-017-04282-8>, <http://www.nature.com/articles/s41598-017-04282-8>, 2017.

- Perroy, R. L., Bookhagen, B., Asner, G. P., and Chadwick, O. A.: Comparison of gully erosion estimates using airborne and ground-based LiDAR on Santa Cruz Island, California, *Geomorphology*, 118, 288 – 300, <https://doi.org/10.1016/j.geomorph.2010.01.009>, <http://www.sciencedirect.com/science/article/pii/S0169555X10000358>, 2010.
- Renard, K. G., Foster, G. R., Weesies, G. A., McCool, D. K., and Yoder, D. C.: Predicting soil erosion by water: a guide to conservation planning with the Revised Universal Soil Loss Equation (RUSLE), Tech. Rep. 703, US Government Printing Office, Washington, DC, [https://www.ars.usda.gov/ARSUserFiles/64080530/rusle/ah\\_703.pdf](https://www.ars.usda.gov/ARSUserFiles/64080530/rusle/ah_703.pdf), 1997.
- Roo, A., , A., Wesseling, C., Jetten, V., and Ritsema, C.: LISEM: A physically-based hydrological and soil erosion model incorporated in a GIS, In: K. Kovar & H.P. Nachtnebel (eds.), *Application of geographic information systems in hydrology and water resources management*. Wallingford (UK), IAHS, 1996. IAHS Publ. 235, pp. 395-403, 1996.
- Schoorl, J., Veldkamp, A., and Bouma, J.: Modeling Water and Soil Redistribution in a Dynamic Landscape Context, *Soil Science Society of American Journal*, 66, 1610–1619, 2002.
- Schoorl, J. M., Sonneveld, M. P. W., and Veldkamp, A.: Three-dimensional landscape process modelling: the effect of DEM resolution, *Earth Surface Processes and Landforms*, 25, 1025–1034, [https://doi.org/10.1002/1096-9837\(200008\)25:9<1025::AID-ESP116>3.0.CO;2-Z](https://doi.org/10.1002/1096-9837(200008)25:9<1025::AID-ESP116>3.0.CO;2-Z), <https://onlinelibrary.wiley.com/doi/abs/10.1002/1096-9837%28200008%2925%3A9%3C1025%3A%3AAID-ESP116%3E3.0.CO%3B2-Z>, 2000.
- Shobe, C. M., Tucker, G. E., and Barnhart, K. R.: The SPACE 1.0 model: A Landlab component for 2-D calculation of sediment transport, bedrock erosion, and landscape evolution, *Geoscientific Model Development*, 10, 4577–4604, <https://doi.org/10.5194/gmd-10-4577-2017>, 2017.
- Sorrie, B. A.: An Inventory of the Significant Natural Areas of Hoke County, North Carolina, Tech. rep., North Carolina Natural Heritage Program, 2004.
- Sorrie, B. A., Gray, J. B., and Crutchfield, P. J.: The Vascular Flora of the Longleaf Pine Ecosystem of Fort Bragg and Weymouth Woods, North Carolina, *Castanea*, 71, 129–161, <https://doi.org/10.2179/05-02.1>, 2006.
- Starek, M. J., Mitasova, H., Hardin, E., Weaver, K., Overton, M., and Harmon, R. S.: Modeling and analysis of landscape evolution using airborne , terrestrial , and laboratory laser scanning, *Geosphere*, 7, 1340–1356, <https://doi.org/10.1130/GES00699.1>, 2011.
- Telling, J., Lyda, A., Hartzell, P., and Glennie, C.: Review of Earth science research using terrestrial laser scanning, *Earth-Science Reviews*, 169, 35 – 68, <https://doi.org/10.1016/j.earscirev.2017.04.007>, <http://www.sciencedirect.com/science/article/pii/S0012825216304433>, 2017.
- Temme, A., Schoorl, J., Claessens, L., and Veldkamp, A.: 2.13 Quantitative Modeling of Landscape Evolution, vol. 2, Elsevier Ltd., <https://doi.org/10.1016/B978-0-12-374739-6.00039-7>, <http://linkinghub.elsevier.com/retrieve/pii/B9780123747396000397>, 2013.
- Thaxton, C. S.: Investigations of grain size dependent sediment transport phenomena on multiple scales, Phd, North Carolina State University, <http://www.lib.ncsu.edu/resolver/1840.16/3339>, 2004.
- Thomas, J. T., Iverson, N. R., Burkart, M. R., and Kramer, L. A.: Long-term growth of a valley-bottom gully, Western Iowa, *Earth Surface Processes and Landforms*, 29, 995–1009, <https://doi.org/10.1002/esp.1084>, 2004.
- Tucker, G., Lancaster, S., Gasparini, N., and Bras, R.: The channel-hillslope integrated landscape development model (CHILD), in: *Landscape erosion and evolution modeling*, pp. 349–388, Springer, Boston, MA, [https://doi.org/10.1007/978-1-4615-0575-4\\_12](https://doi.org/10.1007/978-1-4615-0575-4_12), 2001.
- Webb, R. and Wilshire, H.: Environmental Effects of Off-Road Vehicles: Impacts and Management in Arid Regions, *Environmental Management Series*, Springer New York, <https://doi.org/10.1007/978-1-4612-5454-6>, 1983.

- Willgoose, G.: Mathematical Modeling of Whole Landscape Evolution, *Annual Review of Earth and Planetary Sciences*, 33, 443–459, <https://doi.org/10.1146/annurev.earth.33.092203.122610>, <http://www.annualreviews.org/doi/10.1146/annurev.earth.33.092203.122610>, 2005.
- Wischmeier, W. H., Smith, D. D., Science, U. S., Administration, E., and Station, P. U. A. E.: Predicting Rainfall Erosion Losses: A Guide to Conservation Planning, Tech. rep., Washington, D.C., <https://naldc.nal.usda.gov/download/CAT79706928/>, 1978.
- Yang, S., Guan, Y., Zhao, C., Zhang, C., Bai, J., and Chen, K.: Determining the influence of catchment area on intensity of gully erosion using high-resolution aerial imagery: A 40-year case study from the Loess Plateau, northern China, *Geoderma*, 347, 90 – 102, <https://doi.org/https://doi.org/10.1016/j.geoderma.2019.03.042>, <http://www.sciencedirect.com/science/article/pii/S0016706118312230>, 2019.
- Zahra, T., Paudel, U., Hayakawa, Y., and Oguchi, T.: Knickzone Extraction Tool (KET) – A New ArcGIS toolset for automatic extraction of knickzones from a DEM based on multi-scale stream gradients, *Open Geosciences*, 9, <https://doi.org/10.1515/geo-2017-0006>, 2017.